

# Study on the molecular mechanisms of rifaximin in the treatment of non-alcoholic steatohepatitis based on the *Helicobacter*-DCA-Fxr-Hnf1 $\alpha$ signalling pathway

YI-PENG WAN<sup>1\*</sup>, SHUANG LI<sup>2\*</sup>, DAN LI<sup>1</sup>, XIAO-MEI HUANG<sup>1</sup>, JIAN-HUA WU<sup>1</sup> and JIE JIAN<sup>1</sup>

<sup>1</sup>Department of Gastroenterology, Second Affiliated Hospital of Nanchang University, Nanchang, Jiangxi 330006, P.R. China;

<sup>2</sup>Department of Teaching, Third Affiliated Hospital of Nanchang University, Nanchang, Jiangxi 330008, P.R. China

Received July 26, 2024; Accepted October 24, 2024

DOI: 10.3892/mmr.2024.13407

**Abstract.** Non-alcoholic steatohepatitis (NASH), the more progressive form of non-alcoholic fatty liver disease, has become a major cause of cirrhosis and liver cancer. The aim of the present study was to investigate the anti-NASH effect of the nonabsorbable antibiotic rifaximin and its specific molecular mechanisms. A methionine-choline deficient (MCD) diet was used to induce NASH formation in mice. The mice with NASH were treated with rifaximin to observe its effects on liver fat deposition, hepatocyte inflammation and liver fibrosis. Furthermore, the intestinal microbiota of mice with NASH was analysed by 16S rRNA sequencing and terminal ileal bile acid levels were assessed using liquid chromatography-electrospray ionization-tandem mass spectrometry analysis. Furthermore, the correlation between the intestinal microflora and bile acid levels in the terminal ileum was investigated, and the effects of rifaximin on the intestinal *Helicobacter*-deoxycholic acid (DCA)-farnesoid X receptor (Fxr)-hepatocyte nuclear factor 1 $\alpha$  (Hnf1 $\alpha$ ) signalling pathway were examined. Moreover, analyses of mice after intestinal decontamination with broad-spectrum antibiotics and of hepatocyte-specific Hnf1 $\alpha$  knockout (Hnf1 $\alpha$ <sup>H-KO</sup>) mice were used to elucidate the molecular mechanisms by which rifaximin improves NASH. Notably, treatment with rifaximin markedly ameliorated liver steatosis, hepatocyte inflammation and liver fibrosis in mice with MCD diet-induced NASH. Rifaximin modulated the gut microbiota, especially *Helicobacter hepaticus*,

in mice with NASH. In addition, rifaximin inhibited the intestinal *Helicobacter*-DCA-Fxr-Hnf1 $\alpha$  signalling pathway in mice with NASH. By contrast, rifaximin did not exert an anti-NASH effect on decontamination-treated mice or Hnf1 $\alpha$ <sup>H-KO</sup> mice. Taken together, these results indicated that rifaximin can ameliorate NASH in mice by modulating the *Helicobacter*-DCA-Fxr-Hnf1 $\alpha$  signalling pathway, providing a theoretical basis for the clinical treatment of patients with NASH with rifaximin.

## Introduction

Non-alcoholic fatty liver disease (NAFLD) has become the leading cause of chronic liver disease worldwide, with ~25% of the global population suffering from NAFLD (1). NAFLD includes non-alcoholic fatty liver (NAFL), non-alcoholic steatohepatitis (NASH), liver fibrosis and cirrhosis, and the main early manifestation of NAFLD is hepatic steatosis. As the disease progresses, hepatic steatosis can progress to NASH with liver fibrosis (2,3). After NASH progresses to the middle or advanced stages, cirrhosis or even liver cancer may occur (4). Previous studies have shown that NASH is a pathogenic factor of cirrhosis, hepatocellular carcinoma and other end-stage liver diseases (5,6).

Although the aetiology and pathogenesis of NAFLD are still unknown, a number of studies have indicated that, in addition to insulin resistance and hepatocellular inflammation, changes in the intestinal microflora and liver metabolic genes may be key factors in the occurrence and progression of NAFLD (7,8). The intestine and liver are closely connected, and enterohepatic axis dysbiosis is closely related to the occurrence of numerous liver diseases, including NAFL, NASH, liver fibrosis and cirrhosis (9-11). The metabolites of the intestinal microflora include bile acids, choline, short-chain fatty acids and endogenous intestinal ethanol. Previous studies have shown that abnormal intestinal microflora metabolites can induce the occurrence and development of NAFLD (12-15). Therefore, the treatment of NAFLD by regulating the intestinal microflora and its metabolites has garnered interest (14).

Rifaximin is an intestinal-specific broad-spectrum antibiotic, which is not absorbed by the intestine and is not metabolized by the liver. Rifaximin can improve the intestinal

**Correspondence to:** Professor Jie Jian, Department of Gastroenterology, Second Affiliated Hospital of Nanchang University, 1 Minde Road, Donghu, Nanchang, Jiangxi 330006, P.R. China  
E-mail: jianjie616@163.com

\*Contributed equally

**Key words:** rifaximin, non-alcoholic steatohepatitis, intestinal microbiota, deoxycholic acid, farnesoid X receptor, hepatocyte nuclear factor 1 $\alpha$

microflora and has been approved by the U.S. Food and Drug Administration (FDA) for treating traveller's diarrhoea and hepatic encephalopathy (16,17). It can also effectively improve the abdominal distension and stool characteristics of patients with irritable bowel syndrome (18,19). Clinical studies have confirmed that rifaximin can ameliorate serum endotoxaemia, inhibit proinflammatory factor expression and improve liver function in patients with NASH (20,21). However, the underlying molecular biological mechanisms of rifaximin in treating NASH are still unclear.

The present study aimed to investigate the anti-NASH effect of the nonabsorbable antibiotic rifaximin and its specific molecular mechanisms.

## Materials and methods

**Ethics approval.** Animal health and behaviour were monitored once every 2 days. The mice with methionine-choline deficient (MCD) diet-induced NASH, mice with NASH and intestinal decontamination, and Hnf1 $\alpha$  knockout (Hnf1 $\alpha^{\text{H-KO}}$ ) mice with NASH were sacrificed at the end of 6, 4 and 24 weeks, respectively, and blood (from cardiac puncture), liver, terminal ileum and caecal content samples were collected. The mice were sacrificed by cervical dislocation following the intraperitoneal injection of pentobarbital sodium (>120 mg/kg). Animal welfare was considered, including minimizing suffering and distress, and using the most appropriate dose of anaesthetic. In addition, death was verified by respiratory and cardiac arrest. All animal experiments were approved by the Naval Medical University (approval no. SYXK2021-0075) and Nanchang University (approval no. LL-202303280001).

**NASH mouse model and rifaximin treatment.** A total of 24 male C57BL/6 mice (age, 6 weeks; weight, ~20 g) were purchased from the Shanghai Experimental Center of the Chinese Academy of Sciences and were housed in the Experimental Animal Center of the Second Military Medical University (also known as Naval Medical University, Shanghai, China) or Nanchang University (Nanchang, China) in a specific pathogen-free environment at 24°C and 50% humidity under a 12-h light/dark cycle. The mice were randomly divided into two groups: One group was fed a methionine-choline sufficient (MCS) diet *ad libitum* (n=8), and the other group was fed an MCD diet (Trophic Animal Feed High-tech Co.) *ad libitum* (n=16). After 2 weeks, the mice fed the MCD diet were randomly separated into two groups: The MCD group (n=8) and the MCD + rifaximin group (n=8). The mice in the MCD + rifaximin group were treated with rifaximin (MedChemExpress) by oral gavage (100 mg/kg/day) for 4 weeks (Fig. S1A). The rifaximin dose was chosen based on a previous report (22). The mice in the MCS and MCD groups were fed water according to their body weight for 4 weeks.

**Intestinal decontamination of mice with NASH and rifaximin treatment.** A total of 32 male C57BL/6 mice (age, 6 weeks; weight, ~20 g) were purchased from the Shanghai Experimental Center of the Chinese Academy of Sciences and were housed in the Experimental Animal Center of the Second Military Medical University or Nanchang University in a specific pathogen-free environment at 24°C and 50% humidity under

a 12-h light/dark cycle. The mice were randomly divided into the following four groups: MCD group (n=8), MCD + rifaximin group (n=8), MCD + Abx group (n=8) and MCD + Abx + rifaximin group (n=8). To determine whether rifaximin relies on the intestinal microflora to serve a biological role in mice with NASH, after 1 week of treatment with broad-spectrum antibiotics (ampicillin 1 g/l, neomycin sulfate 1 g/l, metronidazole 1 g/l and vancomycin 0.5 g/l; MedChemExpress), which were added to the drinking water as described previously (23), 6-week-old male C57BL/6 mice in the MCD + Abx + rifaximin group were administered rifaximin (100 mg/kg/day) by oral gavage for 3 weeks. The mice in the MCD + Abx group were administered broad-spectrum antibiotics in their drinking water for 1 week and were then treated with water by oral gavage according to their body weight for 3 weeks. The mice in the MCD group were administered water for 1 week and were then treated with water by oral gavage according to their body weight for 3 weeks. The mice in the MCD + rifaximin group were administered water for 1 week and were then treated with rifaximin (100 mg/kg/day) by oral gavage for 3 weeks. All mice were fed an MCD diet for 4 weeks. Animal health and behaviour were monitored once every 2 days. All mice were sacrificed after being fed an MCD diet for 4 weeks, and blood (from cardiac puncture), liver and terminal ileum samples were collected.

**Generation of hepatocyte-specific Hnf1 $\alpha^{\text{H-KO}}$  mice and rifaximin treatment.** Hnf1 $\alpha^{\text{H-KO}}$  mice were generated by Shanghai Model Organisms Centre, Inc. by crossing mice homozygous for floxed Hnf1 $\alpha$  (Hnf1 $\alpha^{\text{flf}}$ ) with Alb-Cre transgenic mice as described in our previous research (24). Male Hnf1 $\alpha^{\text{H-KO}}$  mice (age, 6 weeks; weight, ~20 g, n=10) were fed a normal chow diet *ad libitum* in a specific pathogen-free environment at 24°C under a 12-h light/dark cycle for 20 weeks to induce NASH, as described in our previous research (24). In addition, the male mice in the Hnf1 $\alpha^{\text{flf}}$  group (age, 6 weeks; weight, ~20 g, n=5) were fed a normal chow diet *ad libitum* for 20 weeks. Subsequently, Hnf1 $\alpha^{\text{H-KO}}$  mice were randomly separated into two groups: The Hnf1 $\alpha^{\text{H-KO}}$  group (n=5) and the Hnf1 $\alpha^{\text{H-KO}}$  + rifaximin group (n=5). The mice in Hnf1 $\alpha^{\text{H-KO}}$  + rifaximin group were administered rifaximin (100 mg/kg/day) by oral gavage for 4 weeks. The mice in the Hnf1 $\alpha^{\text{flf}}$  group and Hnf1 $\alpha^{\text{H-KO}}$  group were treated with water according to their body weight for 4 weeks. Animal health and behaviour were monitored once every 2 days. All mice were sacrificed at the end of 24 weeks, and blood (from cardiac puncture), liver and terminal ileum samples were collected.

**Histology and immunohistochemistry.** Mouse livers that were fixed in 4% paraformaldehyde at 4°C for 24 h were used for frozen sectioning for Oil Red O staining, and those fixed in 10% formalin at room temperature for 24 h were used for paraffin sectioning according to standard procedures. Paraffin-embedded liver sections (4  $\mu$ m) were stained with haematoxylin and eosin (H&E; haematoxylin staining for 5 min at room temperature and eosin staining for 15 sec at room temperature) for histopathological examination. Oil Red O (Sigma-Aldrich; Merck KGaA) staining was performed for 20 min at room temperature to evaluate the degree of hepatocyte steatosis. Sirius red (Leagene; Beijing Regen

Biotechnology Co., Ltd.) staining was performed for 1 h at room temperature for collagen detection. Images were captured using a light microscope (magnifications, x10, x20 and x40). Liver histology was estimated according to the steatosis score, ballooning score, inflammation score and NAFLD activity score (NAS) designed and validated by the NASH-Clinical Research Network (25). Image analysis software Image-Pro Plus 6.0 (Media Cybernetics, Inc.) was used to semi-quantify the intensity of steatosis or collagen deposition according to the percentage of the positive area of Oil Red O staining or Sirius red staining in the corresponding field of liver tissue.

The paraffin-embedded liver sections underwent immunohistochemical staining according to standard procedures. Briefly, liver sections were deparaffinized in xylene and rehydrated in a series of alcohol concentrations. Subsequently, liver sections underwent antigen retrieval (alkali repair; Tris base 0.3 g, EDTA 0.1 g, H<sub>2</sub>O 250 ml) at 100°C for 20 min. They were then soaked in 3% H<sub>2</sub>O<sub>2</sub> for 10 min at room temperature to remove endogenous peroxidase. Liver sections were blocked with 10% goat serum (cat. no. c0265; Beyotime Institute of Biotechnology) at room temperature for 1 h. The slides were incubated overnight at 4°C with primary antibodies against  $\alpha$ -smooth muscle actin ( $\alpha$ -SMA; 1:1,000; cat. no. ab5694; Abcam) and collagen type 1  $\alpha$ 1 (Col1A1; 1:1,000; cat. no. BA0325; Wuhan Boster Biological Technology, Ltd.), followed by incubation with a horseradish peroxidase-linked immunoglobulin G secondary antibody [cat. no. GK500710; reagent A; 1:500; Gene Technology (Shanghai) Co., Ltd.] at room temperature for 1 h. Finally, an GTVision™ III Detection Rabbit/Mouse Kit [cat. no. GK500710; reagent B1; Gene Technology (Shanghai) Co., Ltd.] was used for staining for 3 min at room temperature. Images were captured using a light microscope (magnifications, x10, x20 and x40).

**Reverse transcription-quantitative PCR (RT-qPCR).** Total RNA was extracted from the liver and distal ileum tissues following the standard TRIzol® (Invitrogen; Thermo Fisher Scientific, Inc.) method. Subsequently, 1  $\mu$ g total RNA was used as a template for cDNA synthesis using PrimeScript RT Master Mix (Takara Bio, Inc.) at 37°C for 15 min and 85°C for 30 sec. The transcript levels were detected by qPCR with a SYBR Green PCR Kit (Takara Bio, Inc.). qPCR conditions were as follows: 95°C for 5 min, followed by 40 cycles at 95°C for 30 sec and 60°C for 30 sec. mRNA expression levels were calculated using the  $2^{-\Delta\Delta C_q}$  method and Gapdh was used as the internal reference (26). The primers used are listed in Table I. All reactions were repeated three times.

**Western blot analysis.** Total protein was extracted from the liver tissues using lysis buffer [Tris-HCl (pH 6.8), 5 ml; 20% SDS, 10 ml; glycerol, 9.9 ml] supplemented with phenylmethanesulfonyl fluoride (Beyotime Institute of Biotechnology). The protein concentration was determined using a BCA protein assay kit (Beyotime Institute of Biotechnology). Protein samples were electrophoresed on 10% SDS-PAGE gels and were then electrotransferred onto nitrocellulose membranes (cat. no. HATF29325; MilliporeSigma). After blocking with 5% skim milk in PBS-0.1% Tween, the membranes were incubated with specific primary antibodies overnight at 4°C, followed by incubation with donkey-anti-mouse

or donkey-anti-rabbit secondary antibodies (1:3,000; cat. nos. 926-32212 and 926-32213; IRDye 700- or 800-conjugated; LI-COR Biosciences) for 1 h at room temperature. Finally, the signals were visualized using an Odyssey infrared imaging system (LI-COR Biosciences) at a wavelength of 700 or 800 nm. The densities of the protein bands were semi-quantified using ImageJ 1.8.0 software (National Institutes of Health). Gapdh was used as the internal control. The primary antibodies used were as follows: Ppar $\gamma$  (cat. no. sc-7273; Santa Cruz Biotechnology, Inc.), sterol regulatory element-binding protein 1 (Srebp1; cat. no. ab28481; Abcam),  $\alpha$ -Sma (cat. no. ab5694; Abcam), Hnf1 $\alpha$  (cat. no. ab272693; Abcam) and Gapdh (cat. no. BSAP0063; Bioworld Technology, Inc.).

**Measurement of hydroxyproline content.** The liver hydroxyproline content was measured according to the protocol of the Hydroxyproline Detection Kit (cat. no. A030-2; Nanjing Jiancheng Bioengineering Institute) as described in our previous study (27).

**Bacterial 16S rRNA amplicon sequencing and analysis.** Caecal contents were collected from the mice and immediately frozen at -80°C. Microbial DNA was extracted from the caecal contents using the PF Mag-Bind Stool DNA Kit (cat. no. M9016-02, Omega Bio-Tek, Inc.) according to the manufacturer's instructions. Briefly, 150 mg caecal contents were added to microcentrifuge tubes containing lysis buffer, and 200  $\mu$ l Buffer AL was added to the sample and mixed. The 1.5-ml microcentrifuge tube was used for collecting extracted DNA (centrifugation, 4°C, 13,000 x g, 5 min). The DNA quality was checked by 1% agarose gel electrophoresis. The V3-V4 region of the 16S rRNA gene sequence was PCR-amplified with primers (338 forward, 5'-ACTCCTACGGGAGGCAGCAG-3'; 806 reverse, 5'-GGACTACHVGGGTWTCTAAT-3'). The PCR conditions were as follows: 95°C for 3 min, followed by 27 cycles at 95°C for 30 sec and 55°C for 30 sec. DNA (100 ng) underwent paired end sequencing (sequencing kit: cat. no. NOVA-5144; NEXTflex Rapid DNA-Seq kit; Bioo Scientific Corporation) on the Illumina MiSeq PE300 platform (Illumina, Inc.) using standard protocols by Shanghai Majorbio Bio-pharm Technology Co., Ltd.

The initial raw sequences were clustered into operational taxonomic units (OTUs) of a 97% identity threshold using Usearch (version 7.1) (28). In addition,  $\alpha$  diversity analysis was calculated with mothur index analysis (version v.1.30.2; <http://mothur.org/wiki/calculators>).  $\beta$  diversity analysis was performed using R software (version 3.3.1) (29) for mapping, using FastTree (version 2.1.3 <http://www.microbesonline.org/fasttree/>) for constructing the evolutionary tree, and using FastUniFrac (<http://github.com/biocore/unifrac>) for analysing the distance matrix between samples.  $\alpha$  diversity analysis and  $\beta$  diversity analysis were used to assess the relative abundance of intestinal microflora among the MCS group, MCD group and MCD + rifaximin group. Non-metric multidimensional scaling (NMDS) analysis, Adonis analysis and partial least squares discriminant analysis (PLS-DA) based on amplicon sequence variant were used to show that the overall composition of the intestinal microbiome was significantly altered by different diets. Linear discriminant analysis effect size (LEfSe) analysis was used to estimate the impact of each microbiota

Table I. Primer sequences used for reverse transcription-quantitative PCR.

Gene	Primer sequence
Ppar $\gamma$	Forward: 5'-TCGCTGATGCACTGCCTATG-3' Reverse: 5'-GAGAGGTCCACAGAGCTGATT-3'
CD36	Forward: 5'-GTGGCCTTGCACTCTCTCAT-3' Reverse: 5'-CATCCACCAGTTGCTCCACA-3'
Srebp1c	Forward: 5'-GAAGCTGTCTGGGGTAGCGTCT-3' Reverse: 5'-CTCTCAGGAGAGTTGGCACCTG-3'
$\alpha$ -Sma	Forward: 5'-CTGTCCCTCTATGCCTCTGG-3' Reverse: 5'-AGGGCTGTGATCTCCTTCTG-3'
Colla1	Forward: 5'-TAAAGGGTCATCGTGGCTTC-3' Reverse: 5'-GACGGCTGAGTAGGGAACAC-3'
Fxr	Forward: 5'-TGGGCTCCGAATCCTCTTAGA-3' Reverse: 5'-TGGTCCTCAAATAAGATCCTTGG-3'
Fgf15	Forward: 5'-GCCATCAAGGACGTCAGCA-3' Reverse: 5'-CTTCCTCCGAGTAGCGAATCAG-3'
Shp	Forward: 5'-TCTGCAGGTCGTCCGACTATTC-3' Reverse: 5'-AGGCAGTGGCTGTGAGATGC-3'
Cyp7a1	Forward: 5'-TCATTGCTTCAGGGCTCCTG-3' Reverse: 5'-TGGGCATCTCAAGCAAACAC-3'
Cyp7b1	Forward: 5'-TAGGCATGACGATCCTGAAA-3' Reverse: 5'-TCTCTGGTGAAGTGGACTGAAA-3'
Cyp8b1	Forward: 5'-GATCCGTCGCGGAGATAAGG-3' Reverse: 5'-CGGGTTGAGGAACCGATCAT-3'
Cyp27a1	Forward: 5'-TCTGGCTACCTGCACTTCCT-3' Reverse: 5'-GTGTGTTGGATGTCTGTGCC-3'
Hnf1 $\alpha$	Forward: 5'-ATGACACGGATGACGATGGG-3' Reverse: 5'-GCCATGGGTCCTCCTGAAG-3'
Gapdh	Forward: 5'-ACCCTTAAGAGGGATGCTGC-3' Reverse: 5'-CCCAATACGGCCAAATCCGT-3'

$\alpha$ -Sma,  $\alpha$ -smooth muscle actin; Colla1, collagen type 1  $\alpha$ 1; Fxr, farnesoid receptor X; Srebp1c, sterol regulatory element-binding protein 1c.

species on the difference between the MCD group and the MCD + rifaximin group via linear discriminant analysis. Kruskal-Wallis test and Dunn's test were performed to detect the significant differences in abundance, and the groups with significant differences in abundance were identified.

**Bile acid analysis.** Terminal ileum samples (0.1 g) were mixed with NaOH and acetonitrile and centrifuged (4°C, 5,698 x g, 5 min). After centrifugation, the supernatants were placed in a chromatographic bottle to detect bile acid levels (performed by Shanghai Majorbio Bio-pharm Technology Co., Ltd.). Chlorpropamide was used as an internal standard for bile acid levels. The bile acid concentrations of the terminal ileum samples were qualitatively and quantitatively determined by liquid chromatography-electrospray ionization-tandem mass spectrometry (LC-ESI-MS/MS) analysis method [LC-ESI-MS/MS (UHPLC-Qtrap); Waters Corporation]. The mass spectrometry

system consisted of air curtain gas 40, ion spray voltage of -4,500 V, temperature 550°C, ion source Gas1 50, and ion source Gas2 50. Chromatographic separation was performed using the BEH C18 liquid chromatography column (100x2.1 mm, 1.8  $\mu$ m; Waters Corporation). The sample size was 5  $\mu$ l (flow rate, 0.4 ml/min), and the mobile phases were phase A (0.1% formic acid in water) and phase B (0.1% formic acid in acetonitrile). The bile acid standard was used to identify different bile acid metabolites detected by LC-ESI-MS/MS. Finally, the peak mass spectrum area of the analytical sample was substituted into a linear equation to calculate the concentration of bile acid.

**Biochemical analysis.** Mouse serum was extracted from whole blood via centrifugation at 3,000 rpm for 15 min at 4°C. Alanine transaminase (ALT) and aspartate transaminase (AST) levels in mouse serum were measured using an automated analyser at Shanghai Sipur-Bika Experimental Animal Co., Ltd.

**Statistical analysis.** Data are presented as the mean  $\pm$  SEM. GraphPad Prism 7.0 software (Dotmatics) was used to analyse the experimental data through one-way ANOVA or Kruskal-Wallis test among multiple groups, and two-tailed unpaired Student's t-test or Mann-Whitney test between two groups. The correlation between the gut microbiota and bile acid levels in the terminal ileum was investigated using a nonparametric Spearman's test. Gut microbiota clustering analysis was performed using Pearson's correlation coefficient.  $P < 0.05$  was considered to indicate a statistically significant difference.

## Results

**Rifaximin ameliorates NASH in MCD diet-fed mice.** After 4 weeks of rifaximin treatment, the livers of the MCD + rifaximin group were smoother and moister than those of the MCD group (Fig. 1A). Furthermore, MCD-fed mice had a significant decrease in body weight and increase in liver-to-body weight ratio compared with in the MCS-fed mice, while rifaximin treatment significantly reduced the liver-to-body weight ratio (Fig. 1B). As expected, the MCD diet caused hepatic steatosis and inflammation, eventually leading to steatohepatitis in MCD group mice compared with the MCS group. As shown in Fig. S1B, the body weight of mice in the MCD + rifaximin group did not significantly differ from that of mice in the MCD group. However, H&E staining of liver sections showed decreased lipid deposition, ballooning and interlobular inflammation in the MCD + rifaximin group compared with that in the MCD group, revealing a notable decrease in the severity of hepatic steatosis after rifaximin treatment (Fig. 1C). Additionally, rifaximin treatment significantly decreased the ballooning score, interlobular inflammation score and total NAS (Fig. 1D). Oil red O staining also showed reduced lipid accumulation in the liver after rifaximin treatment (Fig. 1E). Consistent with these findings, the mRNA expression levels of Srebp1, Ppar $\gamma$  and CD36, which are involved in liver lipid synthesis (30), were significantly decreased in the MCD + rifaximin group compared with in the MCD group (Fig. 1F). Moreover, compared with in the MCD group, plasma ALT in the MCD + rifaximin group was significantly lower, and plasma AST exhibited a downward trend, further indicating improvements in liver injury after rifaximin treatment (Fig. 1G). These



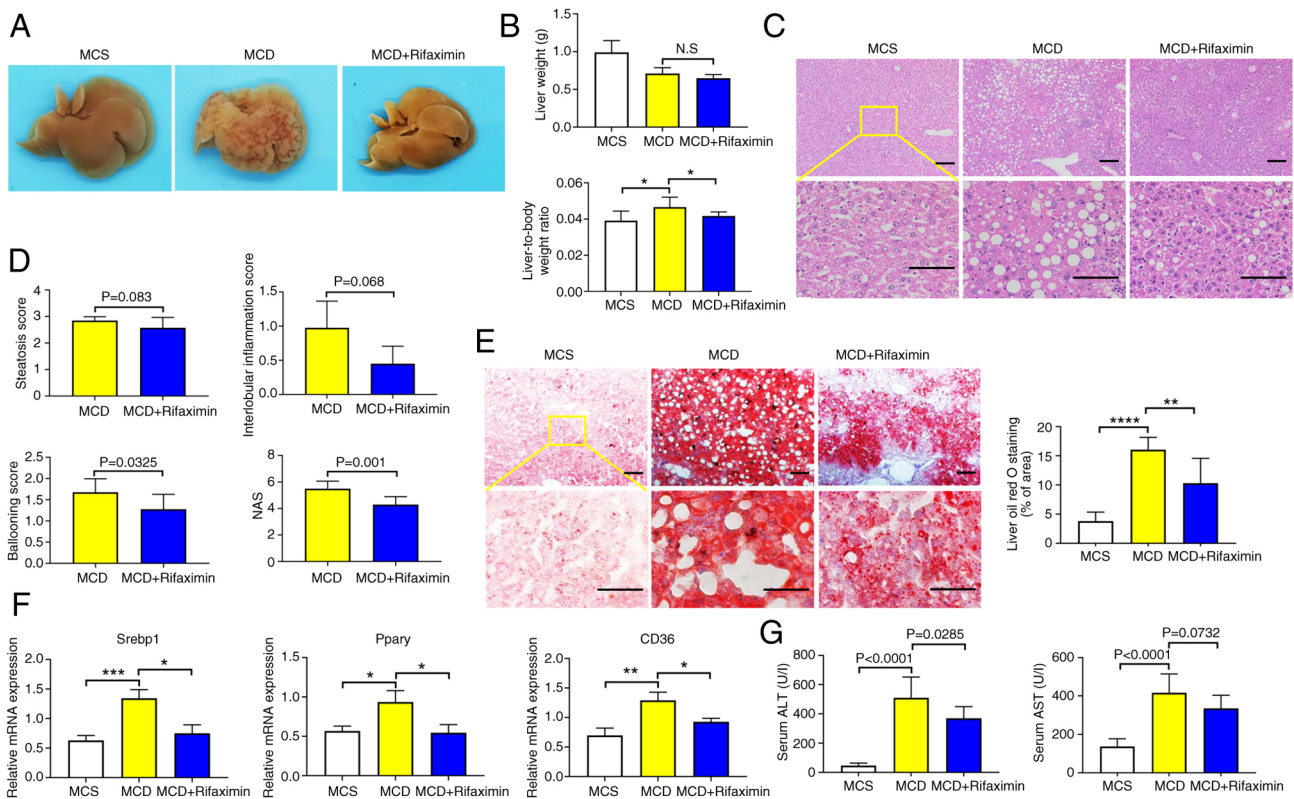


Figure 1. Rifaximin ameliorates non-alcoholic steatohepatitis in MCD diet-fed mice. (A) Photographs of livers in the MCS, MCD and MCD + rifaximin groups. (B) Liver weight, and liver weight to body weight ratio in each group. (C) Haematoxylin and eosin staining of livers in the MCS, MCD and MCD + rifaximin groups. Scale bars, 100  $\mu$ m. (D) Steatosis score, hepatic ballooning score, interlobular inflammation score and NAS. (E) Oil red O staining of livers in the MCS, MCD and MCD + rifaximin groups. Scale bars, 100  $\mu$ m. (F) Srebp1, Ppar $\gamma$  and CD36 mRNA expression levels in mouse livers. (G) Plasma ALT and AST levels in mice. n=8 mice/group. \*P<0.05, \*\*P<0.01, \*\*\*P<0.001, \*\*\*\*P<0.0001. ALT, alanine transaminase; AST, aspartate transaminase; MCD, methionine-choline deficient; MCS, methionine-choline sufficient; NAS, non-alcoholic fatty liver disease activity score; Srebp1, sterol regulatory element-binding protein 1.

results indicated that rifaximin treatment ameliorated NASH in MCD diet-fed mice.

**Rifaximin alleviates MCD diet-induced liver fibrosis in mice with NASH.** With the development of NASH, hepatic stellate cells are activated, and hepatic collagen deposition increases, leading to liver fibrosis (31). Consistent with the findings of previous studies (32,33), the present study revealed that collagen deposition was increased in the livers of mice fed an MCD diet, while rifaximin treatment significantly reduced collagen deposition (Fig. 2A). Moreover, the  $\alpha$ -Sma and Colla1 mRNA and protein expression levels were significantly decreased after rifaximin treatment, as confirmed by immunohistochemistry and RT-qPCR (Fig. 2B-D). Additionally, compared with that in the MCD group, the liver hydroxyproline content in the MCD + rifaximin group was lower, which also indicated that rifaximin treatment alleviated liver fibrosis in mice with MCD diet-induced NASH (Fig. 2E).

**Rifaximin modulates the gut microbiota of mice with MCD diet-induced NASH.** To explore the molecular mechanism by which rifaximin improves NASH, 16S rRNA pyrosequencing was performed on the caecal contents of mice with NASH. It was observed that rifaximin treatment significantly decreased the faecal OTU, Chao1 estimator and Simpson index, but markedly increased the Shannon index, indicating that rifaximin could markedly reduce the total intestinal microflora

and increase bacterial richness (Fig. 3A). As confirmed by plots from NMDS analysis, Adonis analysis and PLS-DA, the gut microbiota composition was substantially reshaped after rifaximin treatment (Figs. 3B, and S2A and B). Notably, LefSe bar analysis, which estimated the magnitude of the influence of the abundance of each component on the differential effect, indicated that the phylum Epsilonbacteraeota was the most abundant gut microbiota associated with group separation between the MCD group and the MCD + rifaximin group (Fig. 3C). Notably, it was observed that, at the phylum level, MCD markedly increased the abundance of Epsilonbacteraeota, the most significantly changed bacteria, while rifaximin treatment significantly decreased the increase in Epsilonbacteraeota abundance in MCD diet-induced NASH mice (Fig. 3D and E). To further determine alterations in the gut microbiota, the intestinal microflora was analysed at the genus level. It was revealed that MCD significantly increased the abundance of *Helicobacter hepaticus*, a member of the Epsilonbacteraeota phylum, while rifaximin treatment markedly decreased the increase in the abundance of *Helicobacter hepaticus* (P=0.0000314; Figs. 3F, 3G and S2C). These results suggested that rifaximin treatment modulated the gut microbiota community, especially *Helicobacter hepaticus*, in the caecal contents of mice with MCD diet-induced NASH.

**Intestinal *Helicobacter-DCA-Fxr* signalling pathway is suppressed after rifaximin treatment.** A close interaction

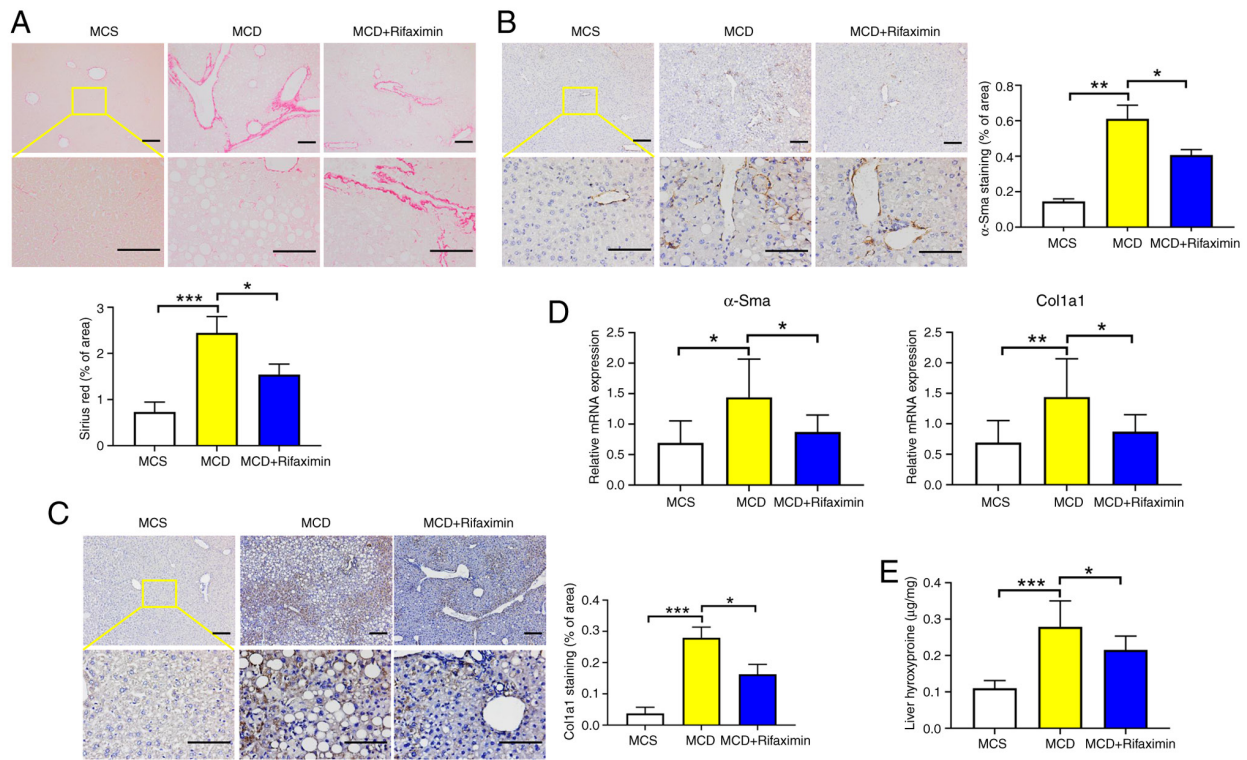


Figure 2. Rifaximin alleviates liver fibrosis in mice with MCD diet-induced non-alcoholic steatohepatitis. (A) Sirius Red staining of livers in each group. Scale bars, 100  $\mu$ m. (B)  $\alpha$ -Sma immunostaining of livers in each group. Scale bars, 100  $\mu$ m. (C) Col1a1 immunostaining of livers in each group. Scale bars, 100  $\mu$ m. (D)  $\alpha$ -Sma and Col1a1 mRNA expression levels of livers in each group. (E) Hydroxyproline content in mouse livers. n=8 mice/group. \* $P$ <0.05, \*\* $P$ <0.01, \*\*\* $P$ <0.001.  $\alpha$ -Sma,  $\alpha$ -smooth muscle actin; Col1a1, collagen type 1  $\alpha$ 1; MCD, methionine-choline deficient; MCS, methionine-choline sufficient.

exists between the intestinal microflora and intestinal bile acids; in particular, bile acids directly inhibit the growth of the gut microbiota. In addition, bile saline hydrolase (BSH), encoded by some intestinal microflora, can hydrolyse bile acids to resist the antibacterial effect of bile acids (34). To evaluate the potential link between rifaximin-induced changes in the intestinal microflora composition and bile acid levels in the terminal ileum, Spearman's correlation analysis was performed. As shown in Fig. 4A, the abundance of *Helicobacter hepaticus*, which was the most significantly altered bacteria in mice with MCD diet-induced NASH, was positively correlated with DCA. Therefore, it was speculated that DCA in the terminal ileum may decrease with decreasing *Helicobacter hepaticus* abundance after rifaximin treatment. As expected, a bile acid assay of the terminal ileum demonstrated that DCA was significantly elevated in mice with MCD diet-induced NASH, whereas rifaximin treatment markedly decreased the increase in DCA (Fig. 4B). In addition, the total bile acid content, conjugated bile acid/unconjugated bile acid ratio, and primary bile acid/second bile acid ratio did not significantly change after rifaximin treatment (Fig. 4C). DCA has been reported to be an intestinal Fxr agonist involved in activating the intestinal Fxr-fibroblast growth factor 15 (Fgf15) signalling pathway to affect liver cholesterol metabolism and bile acid synthesis (35). Therefore, the present study further detected the intestinal Fxr-Fgf15-Cyp7a1 signalling pathway. It was observed that rifaximin treatment significantly downregulated the expression of Fxr and Fgf15 in the distal ileum, but markedly increased Cyp7a1 and Cyp7b1 expression in the liver (Fig. 4D and E), compared with that in the MCD

group. These results indicated that rifaximin may inhibit the intestinal *Helicobacter*-DCA-Fxr signalling pathway.

*Anti-NASH effects of rifaximin are impaired in mice lacking gut microbiota.* To determine whether the anti-NASH effects of rifaximin are mediated through the gut microbiota, the effects of rifaximin on hepatic steatosis, inflammation and fibrosis were assessed in mice with NASH and intestinal decontamination. After 1 week of treatment with broad-spectrum antibiotics (ampicillin 1 g/l, neomycin sulphate 1 g/l, metronidazole 1 g/l and vancomycin 0.5 g/l) in the drinking water, as previously described (23), the mice in the MCD + Abx + rifaximin group were administered rifaximin 100 mg/kg/day by oral gavage for 3 weeks, and the mice in the MCD + Abx group were treated with water by oral gavage according to their body weight for 3 weeks (Fig. 5A). Notably, no further improvement was observed in liver steatosis, hepatocyte ballooning or lobular inflammation after rifaximin treatment in mice with NASH and intestinal decontamination (Fig. 5B and C). In addition, Oil Red O staining showed no further reduction in lipid accumulation in the livers of the MCD + Abx + rifaximin group compared with those of the MCD + Abx group (Fig. 5D). Moreover, the protein expression levels of Ppar $\gamma$  and Srebp1 in the MCD + Abx + rifaximin group were not significantly different from those in the MCD + Abx group (Fig. 5E). Additionally,  $\alpha$ -Sma protein expression was not significantly reduced after rifaximin treatment in mice with NASH and intestinal decontamination (Fig. 5F). These findings indicated that intestinal decontamination could impair the ability of rifaximin to ameliorate hepatic steatosis, inflammation and fibrosis, suggesting that the intestinal

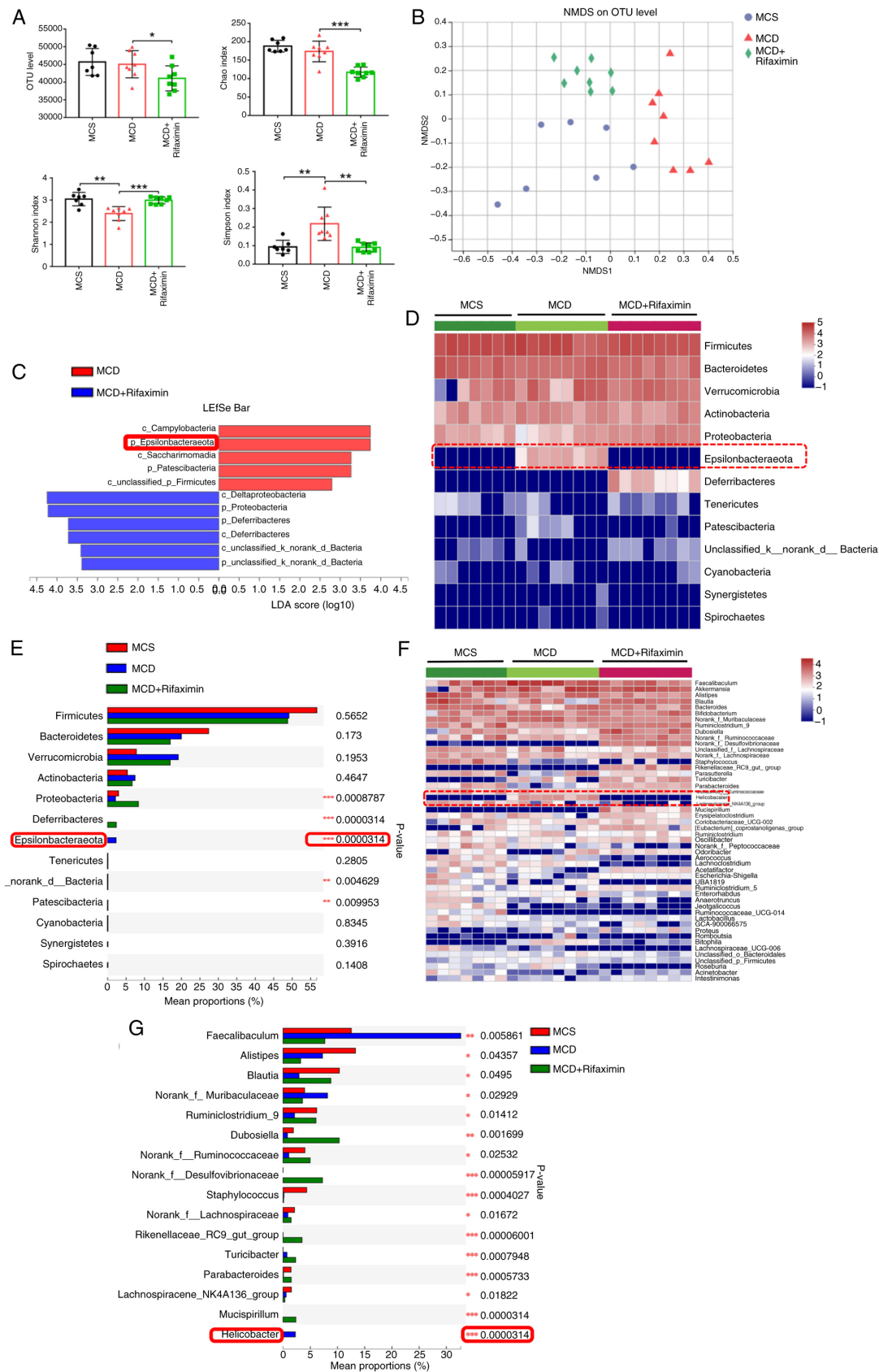


Figure 3. Rifaximin affects the gut microbiota in mice with MCD diet-induced non-alcoholic steatohepatitis. (A) Caecal OTU, Chao index, Simpson index and Shannon index of mice. (B) Separation of samples by MCS, MCD, and MCD with rifaximin gavage was observed via NMDS analysis. (C) Relative abundance of gut microbiota in caecal content identified by LEfSe bar analysis among MCS, MCD and MCD + rifaximin groups. (D) Heatmap of separation at the phylum level of mouse faecal microbiota among the MCS, MCD and MCD + rifaximin groups. (E) Significant difference in mouse faecal microbiota at the phylum level among the MCS, MCD and MCD + rifaximin groups. (F) Heatmap of separation at the genus level of mouse faecal microflora among the MCS, MCD and MCD + rifaximin groups. (G) Significant difference of mouse faecal microbiota at the genus level among the MCS, MCD and MCD + rifaximin groups. Clustering was performed using the Pearson measurement. \* $P < 0.05$ , \*\* $P < 0.01$ , \*\*\* $P < 0.001$ . LDA, linear discriminant analysis; MCD, methionine-choline deficient; MCS, methionine-choline sufficient; NMDS, non-metric multidimensional scaling; OTU, operational taxonomic unit.



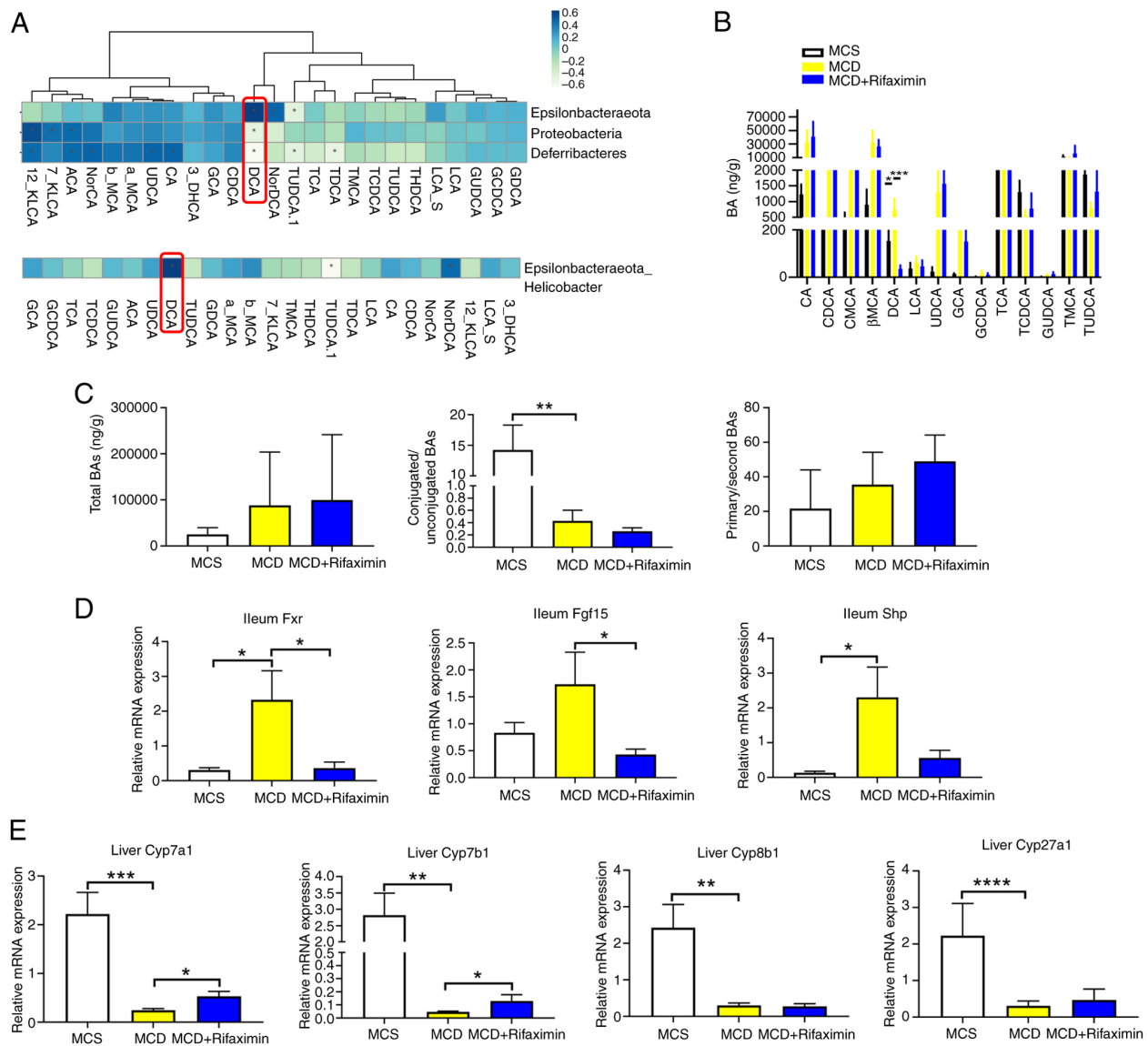


Figure 4. Rifaximin suppresses the *Helicobacter*-DCA-Fxr signalling pathway in MCD diet-fed mice. (A) Correlation analysis of intestinal microflora and BAs in the distal ileum was investigated using nonparametric Spearman's test. (B) BA levels in the distal ileum of mice. (C) Total BAs, conjugated BAs/unconjugated BAs ratio, and primary BAs/secondary BAs ratio in the distal ileum of mice. (D) Expression levels of Fxr, Fgf15 and Shp in the distal ileum. (E) Expression levels of Cyp7a1, Cyp7b1, Cyp8b1, and Cyp27a1 mRNA in the liver. n=8 mice/group. \* $P<0.05$ , \*\* $P<0.01$ , \*\*\* $P<0.001$ , \*\*\*\* $P<0.0001$ . BA, bile acid; DCA, deoxycholic acid; Fgf15, fibroblast growth factor 15; Fxr, farnesoid X receptor; MCD, methionine-choline deficient; MCS, methionine-choline sufficient.

microbiota is required for the ability of rifaximin to ameliorate MCD diet-induced NASH in mice.

**Activation of hepatic *Hnf1a* is required for rifaximin to ameliorate NASH in mice.** The present study revealed that rifaximin could improve bile acid and cholesterol metabolism by regulating the intestinal *Helicobacter*-DCA-Fxr pathway. Therefore, the study aimed to determine how rifaximin specifically affects liver cell function. Our previous study indicated that *Hnf1a*<sup>H-KO</sup> mice spontaneously develop NASH (24). Notably, the present study revealed that rifaximin enhanced liver *Hnf1a* and Fxr mRNA expression compared with that in the MCD group (Fig. S1C). Therefore, it was hypothesized that the activation of hepatic *Hnf1a* may be required for rifaximin to ameliorate NASH in mice. To confirm this hypothesis, *Hnf1a*<sup>H-KO</sup> mice were generated by crossing mice homozygous for *Hnf1a*<sup>fl/fl</sup> with Alb-Cre transgenic mice (Fig. 6A). Male *Hnf1a*<sup>H-KO</sup> mice were fed a normal chow

diet for 20 weeks to induce NASH, then treated with rifaximin by oral gavage for 4 weeks (Fig. 6B). As shown in Fig. 6C, the protein expression levels of *Hnf1a* in the *Hnf1a*<sup>H-KO</sup> group and *Hnf1a*<sup>H-KO</sup> + rifaximin groups were lower than those in *Hnf1a*<sup>fl/fl</sup> group. Notably, it was observed that liver steatosis, hepatocyte ballooning, lobular inflammation and NAS in the *Hnf1a*<sup>H-KO</sup> + rifaximin group were not significantly different from those in the *Hnf1a*<sup>H-KO</sup> group (Fig. 6D and E). In addition, no further improvement in lipid accumulation was observed after rifaximin treatment in mice with *Hnf1a* knockout (Fig. 6F). Moreover, the protein expression levels of Ppar $\gamma$  and Srebp1 in the *Hnf1a*<sup>H-KO</sup> + rifaximin group were not significantly different from those in the *Hnf1a*<sup>H-KO</sup> group (Fig. 6G). Additionally,  $\alpha$ -Sma protein expression was not significantly reduced after rifaximin treatment in *Hnf1a*<sup>H-KO</sup> mice with NASH (Fig. 6H). Based on these results, it was indicated that the anti-NASH biological effects of rifaximin depend on the activation of liver *Hnf1a*.

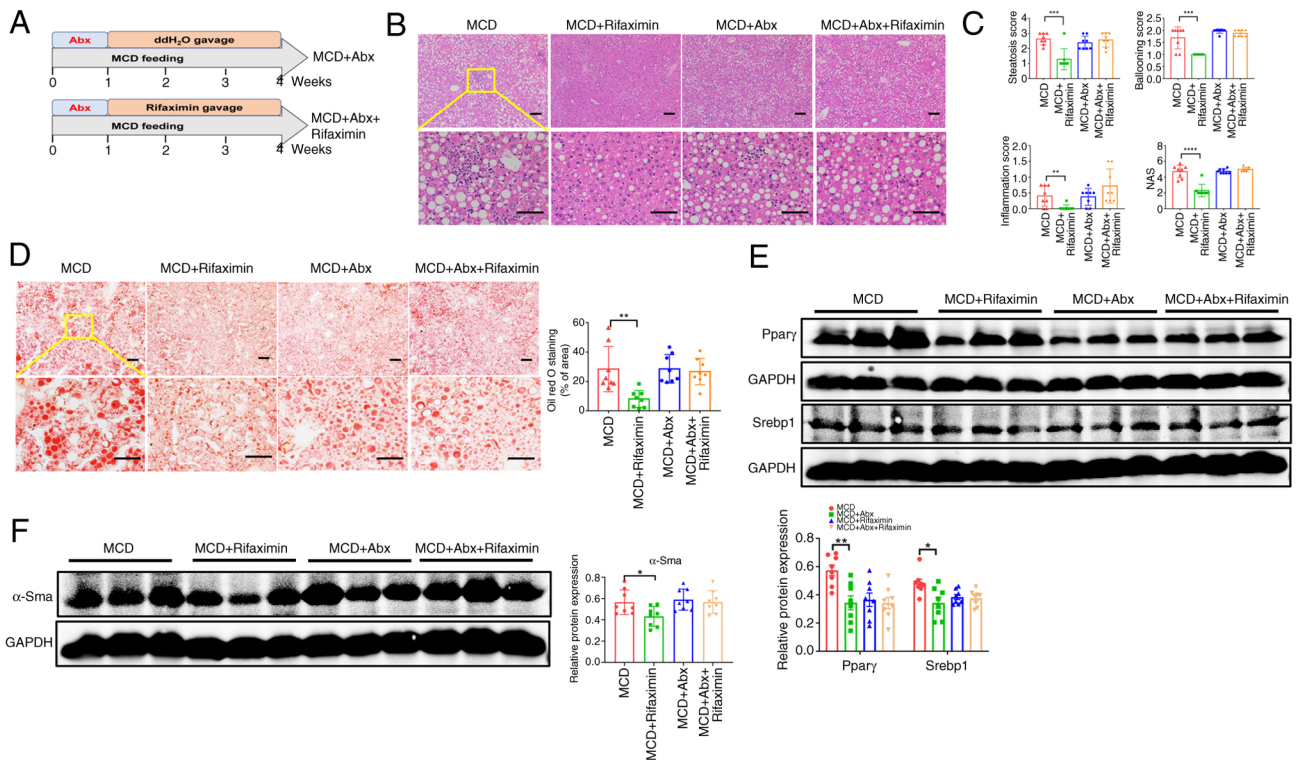


Figure 5. Anti-NASH effects of rifaximin are impaired in mice lacking gut microbiota. (A) Schematic illustration of the experimental design of intestinal decontamination in mice with NASH. (B) Haematoxylin and eosin staining of livers in the MCD, MCD + rifaximin, MCD + Abx and MCD + Abx + rifaximin groups. Scale bars, 100  $\mu$ m. (C) Steatosis score, hepatic ballooning score, interlobular inflammation score and NAS. (D) Oil red O staining for livers of mice in each group. Scale bars, 100  $\mu$ m. (E) Ppar $\gamma$  and Srebp1 protein expression levels in mouse livers. (F)  $\alpha$ -Sma protein expression levels in the livers in each group. n=8 mice/group. \*P<0.05, \*\*P<0.01, \*\*\*P<0.001, \*\*\*\*P<0.0001.  $\alpha$ -Sma,  $\alpha$ -smooth muscle actin; MCD, methionine-choline deficient; MCS, methionine-choline sufficient; NASH, non-alcoholic steatohepatitis; NAS, non-alcoholic fatty liver disease activity score; Srebp1, sterol regulatory element-binding protein 1.

On the basis of these results, it could be concluded that the anti-NASH biological effects of rifaximin depend on modulation of the intestinal *Helicobacter*-DCA-Fxr-Hnf1 $\alpha$  signalling pathway.

## Discussion

Although previous clinical studies have indicated that rifaximin can ameliorate serum endotoxaemia and inhibit proinflammatory factor expression in patients with NASH (20,21), the potential molecular biological mechanisms of rifaximin in treating NASH are currently unknown. The present study showed that mice in the MCD + rifaximin group had significantly lower liver-to-body weight ratio than mice in the MCD group. Moreover, rifaximin treatment significantly improved liver lipid deposition, hepatocyte ballooning and lobular inflammation. During the development of NASH, liver inflammation persists, leading to liver cell damage and increased ALT levels (36). The present results showed that rifaximin treatment reduced the serum ALT levels in mice with NASH and improved their liver function. Srebp1 is an important transcription factor for liver lipid metabolism, which serves a crucial role in the occurrence and development of NASH (37). Ppar $\gamma$  is a ligand-activated receptor in the nuclear hormone receptor family that is involved in regulating cell proliferation, inflammation, and lipid and glucose homeostasis (38). Consistent with previous research results, the present study indicated that the expression levels of Srebp1 and Ppar $\gamma$  were upregulated in mice with NASH, whereas rifaximin

treatment significantly decreased the increased levels of Srebp1 and Ppar $\gamma$ , and inhibited liver lipid metabolism.

With the development of NASH,  $\alpha$ -Sma expression in the liver is upregulated, red collagen deposition increases and liver fibrosis occurs (33). The present study showed that the expression levels of  $\alpha$ -Sma and Colla1 in the liver of the NASH group were markedly upregulated, and red collagen deposition and liver hydroxyproline content were significantly increased. Notably, rifaximin treatment markedly decreased the increase in  $\alpha$ -Sma and Colla1, and reduced red collagen deposition and liver hydroxyproline content. These results indicated that rifaximin treatment may significantly alleviate MCD diet-induced liver fibrosis in mice with NASH.

The interaction between the intestinal microflora and host can affect the circadian rhythm of tissues and organs, which in turn changes metabolic homeostasis (39). It has previously been demonstrated that gut microbiota dysbiosis is closely related to the occurrence and development of NAFLD (40). Rifaximin is an intestinal-specific broad-spectrum antibiotic, which is not absorbed by the intestine and is not metabolized by the liver. Most of the time, rifaximin is used as a probiotic that regulates the gut flora. It has been approved by the U.S. FDA for the treatment of traveller's diarrhoea and hepatic encephalopathy due to its ability to improve intestinal microflora imbalance (16,18). Therefore, in the present study, mouse caecal content samples were collected for bacterial 16S rRNA gene sequencing and the potential involvement of the intestinal microflora in mediating MCD diet-induced NASH was explored. The results revealed that MCD significantly



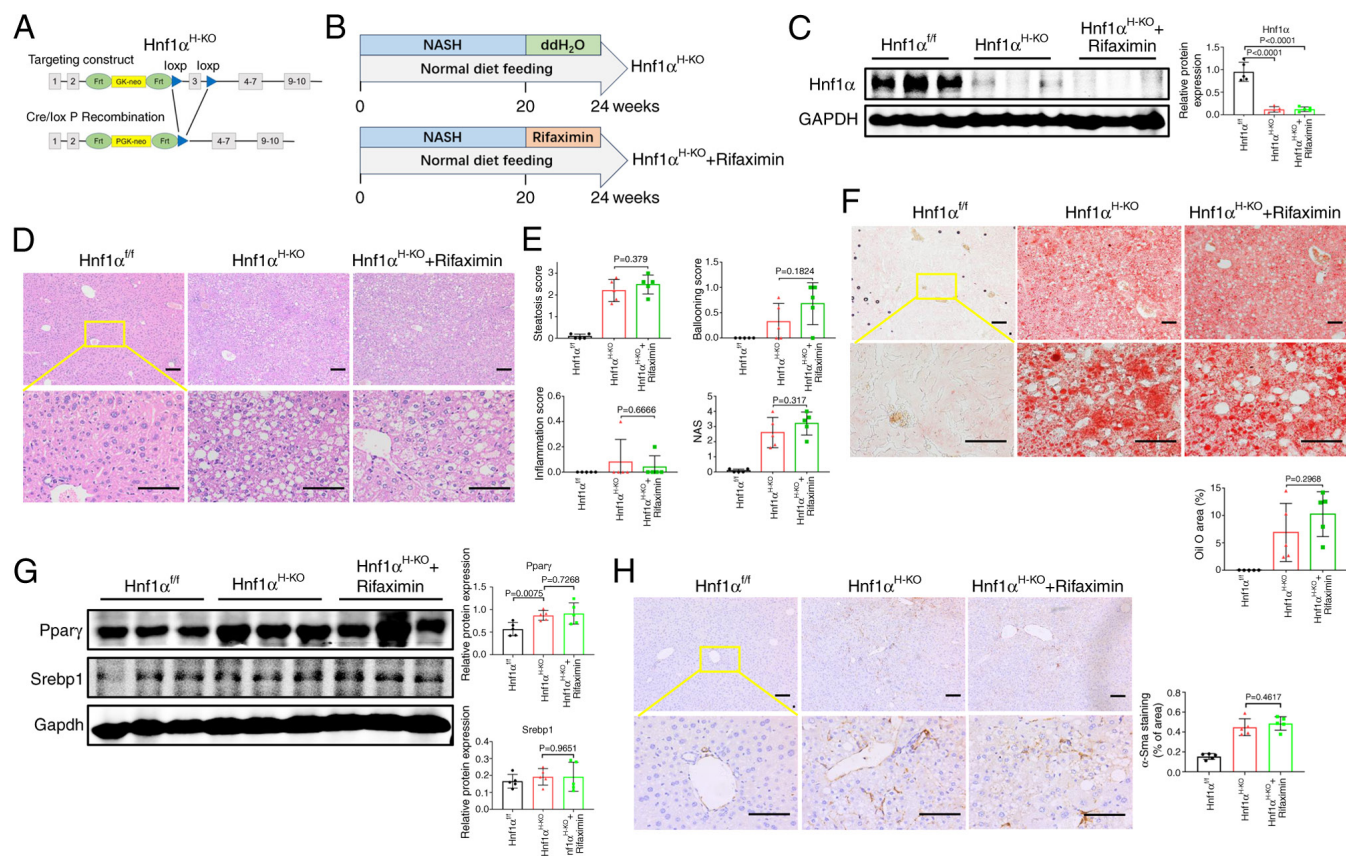


Figure 6. Activation of hepatic *Hnf1α* is required for rifaximin to ameliorate NASH in mice. (A) *Hnf1α*<sup>H-KO</sup> NASH mice were established. (B) Schematic illustration of the experimental design. (C) *Hnf1α* protein expression levels in the mouse livers of each group. (D) Haematoxylin and eosin staining of livers in each group. Scale bars, 100 μm. (E) Steatosis score, hepatic ballooning score, interlobular inflammation score and NAS. (F) Oil red O staining for livers of mice in each group. Scale bars, 100 μm. (G) *Pparγ* and *Srebp1* protein expression levels in the livers of each group. (H) α-Sma protein expression level in the livers in each group. n=5 mice/group. α-Sma, α-smooth muscle actin; *Hnf1α*, hepatocyte nuclear factor 1α; *Hnf1α*<sup>H-KO</sup>, floxed *Hnf1α*; *Hnf1α*<sup>H-KO</sup>, hepatocyte-specific *Hnf1α* knockout; MCD, methionine-choline deficient; MCS, methionine-choline sufficient; NASH, non-alcoholic steatohepatitis; NAS, non-alcoholic fatty liver disease activity score; *Srebp1*, sterol regulatory element-binding protein 1.

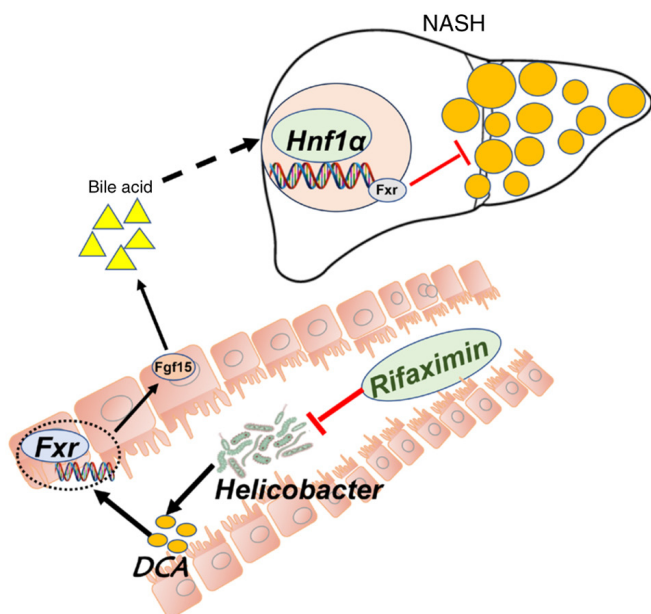


Figure 7. Illustration of the molecular mechanism of rifaximin in treating NASH in mice. Inhibition of the *Helicobacter*-DCA-Fxr-*Hnf1α* signalling pathway is required for rifaximin to ameliorate NASH in mice. DCA, deoxycholic acid; Fgf15, fibroblast growth factor 15; Fxr, farnesoid X receptor; *Hnf1α*, hepatocyte nuclear factor 1α; NASH, non-alcoholic steatohepatitis.

decreased the faecal OTU, Chao1 index and Simpson index, but markedly increased the Shannon index, indicating that rifaximin can markedly reduce the total intestinal microflora and increase bacterial richness. Furthermore, it was observed that, compared with that in the MCS group, *Helicobacter hepaticus* was the most significantly affected bacteria in the MCD group, while rifaximin treatment markedly decreased the increase in *Helicobacter hepaticus*. In addition, Epsilonbacteraeota was one of the most significantly changed bacteria between the MCD group and the MCD + rifaximin group; however, there was no difference in Epsilonbacteraeota between the MCS group and the MCD group. A previous study reported that *Helicobacter hepaticus* could promote hepatitis development by regulating the Fxr signalling pathway (41). Therefore, the present study speculated that rifaximin may improve liver inflammation by decreasing the abundance of *Helicobacter hepaticus*.

There is a close interaction between the gut microbiota and intestinal bile acids. On the one hand, bile acids directly inhibit the growth of the intestinal microflora due to their antibacterial effect, whereas on the other hand, BSH, which is encoded by some intestinal microflora, can hydrolyse bile acids to resist their antibacterial effect (34). Therefore, Spearman's correlation analysis was performed between the intestinal microflora and bile acid levels in the terminal ileum. Notably, it was observed

that *Helicobacter hepaticus* abundance was significantly positively correlated with DCA. Therefore, a full-spectrum test of bile acids was performed in the terminal ileum. As expected, the results showed that DCA in the terminal ileum was significantly decreased following rifaximin treatment. There is evidence that DCA is an intestinal Fxr agonist, which activates the intestinal Fxr-Fgf15 signalling pathway, and affects liver cholesterol and bile acid metabolism (35). Therefore, the present study further detected the intestinal Fxr-Fgf15-Cyp7a1 signalling pathway. It was observed that rifaximin significantly downregulated the expression of Fxr and Fgf15 in the distal ileum, but markedly increased Cyp7a1 and Cyp7b1 expression in the liver. Based on these results, it could be speculated that rifaximin may inhibit the growth of *Helicobacter hepaticus* and reduce DCA in the distal ileum, thereby inhibiting the intestinal Fxr-Fgf15 signalling pathway to improve liver cholesterol and bile acid metabolism in mice with NASH.

To further confirm that rifaximin relies on the intestinal microbiota to serve a molecular biological role in preventing NASH, mice with NASH were first treated with broad-spectrum antibiotics for intestinal decontamination and were then treated with rifaximin. As expected, no further improvement in liver steatosis, hepatocyte ballooning or lobular inflammation was observed in the MCD + Abx + rifaximin group compared with that in the MCD + Abx group. Moreover, the expression levels of Ppar $\gamma$ ,  $\alpha$ -Sma and Colla1 were not significantly reduced following rifaximin treatment in mice with NASH and intestinal decontamination. These findings indicated that intestinal decontamination may impair the ability of rifaximin to ameliorate hepatic inflammation and fibrosis, suggesting that the intestinal microbiota is required for the ability of rifaximin to ameliorate MCD diet-induced NASH in mice.

Hnf1 $\alpha$  is a liver-enriched transcription factor that modulates liver fatty acid binding protein function to affect liver fatty acid transport and lipid metabolism (42). A previous study revealed that Hnf1 $\alpha$  could regulate liver Fxr expression, and affect lipid and cholesterol metabolism by directly binding to the liver Fxr transcription factor (43). *In vivo* experiments in mice also confirmed that activation of the Hnf1 $\alpha$ -Fxr signalling pathway can regulate liver bile acid metabolism and inhibit the formation of cholesterol stones (44). Furthermore, our previous study indicated that Hnf1 $\alpha$ <sup>H-KO</sup> mice develop spontaneous NASH (24). Notably, the present study revealed that rifaximin activated liver Hnf1 $\alpha$  expression. Therefore, it was speculated that activation of hepatic Hnf1 $\alpha$  was required for rifaximin to ameliorate NASH in mice. To confirm this hypothesis, Hnf1 $\alpha$ <sup>H-KO</sup> mice with NASH were treated with rifaximin. Subsequently, it was observed that liver lipid deposition, liver inflammation and liver fibrosis were not significantly improved after rifaximin treatment when Hnf1 $\alpha$  was knocked out. These findings confirmed that the anti-NASH biological effects of rifaximin depend on the activation of liver Hnf1 $\alpha$ .

In conclusion, rifaximin can inhibit the proliferation of intestinal *Helicobacter hepaticus*, thereby decreasing the DCA in the terminal ileum and inhibiting the intestinal Fxr-Fgf15 signalling pathway. With inhibition of the intestinal Fxr-Fgf15 signalling pathway, increased Cyp7a1 and Cyp7b1 in the liver can further activate the liver Hnf1 $\alpha$ -Fxr signalling pathway and improve liver lipid metabolism, ultimately

inhibiting the progression of NASH (Fig. 7). However, humans and mice have different physiological structures. The present study revealed that rifaximin can improve lipid and cholesterol metabolism in mice with NASH; however, it is unclear whether it has the same biological effect on patients with NASH. In future studies, different doses of rifaximin will be administered to patients with NASH to observe the clinical therapeutic effect. The findings of the present study provide a theoretical basis for the clinical treatment of rifaximin in patients with NASH.

### Acknowledgements

The authors would like to thank Professor Mei-Tong Nie (Department of Gastroenterology, Shanghai East Hospital, Tongji University School of Medicine) for providing their assistance in submitting the data to a public curated database.

### Funding

This work was supported by the National Natural Science Foundation of China (grant no. 82360123) and the Natural Science Foundation of Jiangxi Province (grant nos. 20232BAB206017 and 20242BAB20355).

### Availability of data and materials

The sequencing data generated in the present study may be found in the BioProject database under accession number PRJNA1172135 or at the following URL: <https://www.ncbi.nlm.nih.gov/bioproject/?term=PRJNA1172135>. The other data generated in the present study may be requested from the corresponding author.

### Authors' contributions

JJ conceived and designed the experiments. YPW and SL wrote the manuscript. YPW, SL, DL and XMH performed the experiments. JHW analysed data. YPW and JJ revised the manuscript. YPW and JJ confirm the authenticity of all the raw data. All authors read and approved the final version of the manuscript.

### Ethics approval and consent to participate

The animal experiments were initially performed at Naval Medical University and later at Nanchang University. All animal experiments were performed in accordance with the National Institute of Health Guide for the Care and Use of Laboratory Animals, and were approved by the Naval Medical University (approval no. SYXK2021-0075) and Nanchang University (approval no. LL-202303280001).

### Patient consent for publication

Not applicable.

### Competing interests

The authors declare that they have no competing interests.

## References

1. Younossi Z, Tacke F, Arrese M, Chander Sharma B, Mostafa I, Bugianesi E, Wai-Sun Wong V, Yilmaz Y, George J, Fan J and Vos MB: Global perspectives on nonalcoholic fatty liver disease and nonalcoholic Steatohepatitis. *Hepatology* 69: 2672-2682, 2019.
2. Friedman SL, Neuschwander-Tetri BA, Rinella M and Sanyal AJ: Mechanisms of NAFLD development and therapeutic strategies. *Nat Med* 24: 908-922, 2018.
3. Schuster S, Cabrera D, Arrese M and Feldstein AE: Triggering and resolution of inflammation in NASH. *Nat Rev Gastroenterol Hepatol* 15: 349-364, 2018.
4. Zhang X, Coker OO, Chu ES, Fu K, Lau HCH, Wang YX, Chan AWH, Wei H, Yang X, Sung JY and Yu J: Dietary cholesterol drives fatty liver-associated liver cancer by modulating gut microbiota and metabolites. *Gut* 70: 761-774, 2021.
5. De Sousa SM Dr and Norman RJ Prof: Metabolic syndrome, diet and exercise. *Best Pract Res Clin Obstet Gynaecol* 37: 140-151, 2016.
6. Kim D, Tournas A and Kim WR: Nonalcoholic fatty liver disease and metabolic syndrome. *Clin Liver Dis* 22: 133-140, 2018.
7. Sharpston SR, Ajmera V and Loomba R: Emerging role of the gut microbiome in nonalcoholic fatty liver disease: From composition to function. *Clin Gastroenterol Hepatol* 17: 296-306, 2019.
8. Ponziani FR, Bhoori S, Castelli C, Putignani L, Rivoltini L, Del Chierico F, Sanguinetti M, Morelli D, Paroni Sterbini F, Petito V, *et al*: Hepatocellular carcinoma is associated with gut microbiota profile and inflammation in nonalcoholic fatty liver disease. *Hepatology* 69: 107-120, 2019.
9. Grabherr F, Grander C, Effenberger M, Adolph TE and Tilg H: Gut dysfunction and non-alcoholic fatty liver disease. *Front Endocrinol (Lausanne)* 10: 611, 2019.
10. Sun L, Pang Y, Wang X, Wu Q, Liu H, Liu B, Liu G, Ye M, Kong W and Jiang C: Ablation of gut microbiota alleviates obesity-induced hepatic steatosis and glucose intolerance by modulating bile acid metabolism in hamsters. *Acta Pharm Sin B* 9: 702-710, 2019.
11. Jasirwan COM, Lesmana CRA, Hasan I, Sulaiman AS and Gani RA: The role of gut microbiota in non-alcoholic fatty liver disease: pathways of mechanisms. *Biosci Microbiota Food Health* 38: 81-88, 2019.
12. Chávez-Talavera O, Tailleux A, Lefebvre P and Staels B: Bile acid control of metabolism and inflammation in obesity, type 2 diabetes, dyslipidemia, and nonalcoholic fatty liver disease. *Gastroenterology* 152: 1679-1694.e3, 2017.
13. Corbin KD and Zeisel SH: Choline metabolism provides novel insights into nonalcoholic fatty liver disease and its progression. *Curr Opin Gastroenterol* 28: 159-165, 2012.
14. Liu HY, Walden TB, Cai D, Ahl D, Bertilsson S, Phillipson M, Nyman M and Holm L: Dietary fiber in bilberry ameliorates pre-obesity events in rats by regulating lipid depot, cecal short-chain fatty acid formation and microbiota composition. *Nutrients* 11: 1350, 2019.
15. Zhu L, Baker SS, Gill C, Liu W, Alkhoury R, Baker RD and Gill SR: Characterization of gut microbiomes in nonalcoholic steatohepatitis (NASH) patients: A connection between endogenous alcohol and NASH. *Hepatology* 57: 601-609, 2013.
16. Coronel-Castillo CE, Contreras-Carmona J, Frati-Munari AC, Uribe M and Méndez-Sánchez N: Efficacy of rifaximin in the different clinical scenarios of hepatic encephalopathy. *Rev Gastroenterol Mex (Engl Ed)* 85: 56-68, 2020 (In English, Spanish).
17. Chautant F, Guillaume M, Robic MA, Cadranet JF, Peron JM, Lison H, Cool C, Bureau C and Duhalde V: Lessons from 'real life experience' of rifaximin use in the management of recurrent hepatic encephalopathy. *World J Hepatol* 12: 10-20, 2020.
18. Fodor AA, Pimentel M, Chey WD, Lembo A, Golden PL, Israel RJ and Carroll IM: Rifaximin is associated with modest, transient decreases in multiple taxa in the gut microbiota of patients with diarrhoea-predominant irritable bowel syndrome. *Gut Microbes* 10: 22-33, 2019.
19. Shah ED, Saini SD and Chey WD: Value-based pricing for rifaximin increases access of patients with irritable bowel syndrome with diarrhea to therapy. *Clin Gastroenterol Hepatol* 17: 2687-2695.e11, 2019.
20. Abdel-Razik A, Mousa N, Shabana W, Refaey M, Elzeheery R, Elhelaly R, Zalata K, Abdelsalam M, Eldeeb AA, Awad M, *et al*: Rifaximin in nonalcoholic fatty liver disease: Hit multiple targets with a single shot. *Eur J Gastroenterol Hepatol* 30: 1237-1246, 2018.
21. Gangarapu V, Ince AT, Baysal B, Kayar Y, Kılıç U, Gök Ö, Uysal Ö and Şentürk H: Efficacy of rifaximin on circulating endotoxins and cytokines in patients with nonalcoholic fatty liver disease. *Eur J Gastroenterol Hepatol* 27: 840-845, 2015.
22. Yang L, Liu B, Zheng J, Huang J, Zhao Q, Liu J, Su Z, Wang M, Cui Z, Wang T, *et al*: Rifaximin alters intestinal microbiota and prevents progression of ankylosing spondylitis in mice. *Front Cell Infect Microbiol* 9: 44, 2019.
23. Zhu Y, He C, Li X, Cai Y, Hu J, Liao Y, Zhao J, Xia L, He W, Liu L, *et al*: Gut microbiota dysbiosis worsens the severity of acute pancreatitis in patients and mice. *J Gastroenterol* 54: 347-358, 2019.
24. Ni Q, Ding K, Wang KQ, He J, Yin C, Shi J, Zhang X, Xie WF and Shi YQ: Deletion of HNF1 $\alpha$  in hepatocytes results in fatty liver-related hepatocellular carcinoma in mice. *FEBS Lett* 591: 1947-1957, 2017.
25. Kleiner DE, Brunt EM, Van Natta M, Behling C, Contos MJ, Cummings OW, Ferrell LD, Liu YC, Torbenson MS, Unalp-Arida A, *et al*: Design and validation of a histological scoring system for nonalcoholic fatty liver disease. *Hepatology* 41: 1313-1321, 2005.
26. Livak KJ and Schmittgen TD: Analysis of relative gene expression data using real-time quantitative PCR and the 2(-Delta Delta C(T)) method. *Methods* 25: 402-408, 2001.
27. Yue HY, Yin C, Hou JL, Zeng X, Chen YX, Zhong W, Hu PF, Deng X, Tan YX, Zhang JP, *et al*: Hepatocyte nuclear factor 4 $\alpha$  attenuates hepatic fibrosis in rats. *Gut* 59: 236-246, 2010.
28. Nie Y, Liu Q, Zhang W, Wan Y, Huang C and Zhu X: Ursolic acid reverses liver fibrosis by inhibiting NOX4/NLRP3 inflammatory pathways and bacterial dysbiosis. *Gut Microbes* 13: 1972746, 2021.
29. R Core Team. R: A language and environment for statistical computing. R Foundation for Statistical Computing, Vienna, Austria, 2021.
30. Quan T, Zhou F, Chen H, Jian L, Yang Y, Xia F, Xiang S, Zhou B and Li S: Ficus hirta Vahl. Ameliorates nonalcoholic fatty liver disease through regulating lipid metabolism and gut microbiota. *Oxid Med Cell Longev* 2022: 3474723, 2022.
31. Mukherjee S, Zhelnin L, Sanfiz A, Pan J, Li Z, Yarde M, McCarty J and Jarai G: Development and validation of an in vitro 3D model of NASH with severe fibrotic phenotype. *Am J Transl Res* 11: 1531-1540, 2019.
32. Kumar S, Duan Q, Wu R, Harris EN and Su Q: Pathophysiological communication between hepatocytes and non-parenchymal cells in liver injury from NAFLD to liver fibrosis. *Adv Drug Deliv Rev* 176: 113869, 2021.
33. Huang R, Guo F, Li Y, Liang Y, Li G, Fu P and Ma L: Activation of AMPK by triptolide alleviates nonalcoholic fatty liver disease by improving hepatic lipid metabolism, inflammation and fibrosis. *Phytomedicine* 92: 153739, 2021.
34. Begley M, Gahan CGM and Hill C: The interaction between bacteria and bile. *FEMS Microbiol Rev* 29: 625-651, 2005.
35. de Aguiar Vallim TQ, Tarling EJ and Edwards PA: Pleiotropic roles of bile acids in metabolism. *Cell Metab* 17: 657-669, 2013.
36. Honda T, Ishigami M, Luo F, Lingyun M, Ishizu Y, Kuzuya T, Hayashi K, Nakano I, Ishikawa T, Feng GG, *et al*: Branched-chain amino acids alleviate hepatic steatosis and liver injury in choline-deficient high-fat diet induced NASH mice. *Metabolism* 69: 177-187, 2017.
37. Zhang L, Li HX, Pan WS, Khan FU, Qian C, Qi-Li FR and Xu X: Novel hepatoprotective role of Leonurine hydrochloride against experimental non-alcoholic steatohepatitis mediated via AMPK/SREBP1 signalling pathway. *Biomed Pharmacother* 110: 571-581, 2019.
38. Cheng S, Qian K, Wang Y, Wang G, Liu X, Xiao Y and Wang X: PPAR $\gamma$  inhibition regulates the cell cycle, proliferation and motility of bladder cancer cells. *J Cell Mol Med* 23: 3724-3736, 2019.
39. Voigt RM, Summa KC, Forsyth CB, Green SJ, Engen P, Naqib A, Vitaterna MH, Turek FW and Keshavarzian A: The circadian clock mutation promotes intestinal dysbiosis. *Alcohol Clin Exp Res* 40: 335-347, 2016.
40. Canfora EE, Meex RCR, Venema K and Blaak EE: Gut microbial metabolites in obesity, NAFLD and T2DM. *Nat Rev Endocrinol* 15: 261-273, 2019.
41. Swennes AG, Sheh A, Parry NMA, Muthupalani S, Lertpiriyapong K, García A and Fox JG: *Helicobacter hepaticus* infection promotes hepatitis and preneoplastic foci in farnesoid X receptor (FXR) deficient mice. *PLoS One* 9: e106764, 2014.

42. Qadri I, Hu LJ, Iwahashi M, Al-Zuabi S, Quattrochi LC and Simon FR: Interaction of hepatocyte nuclear factors in transcriptional regulation of tissue specific hormonal expression of human multidrug resistance-associated protein 2 (abcc2). *Toxicol Appl Pharmacol* 234: 281-292, 2009.
43. Xiong X, Wang X, Lu Y, Wang E, Zhang Z, Yang J, Zhang H and Li X: Hepatic steatosis exacerbated by endoplasmic reticulum stress-mediated downregulation of FXR in aging mice. *J Hepatol* 60: 847-854, 2014.
44. Purushotham A, Xu Q, Lu J, Foley JF, Yan X, Kim DH, Kemper JK and Li X: Hepatic deletion of SIRT1 decreases hepatocyte nuclear factor 1 $\alpha$ /farnesoid X receptor signaling and induces formation of cholesterol gallstones in mice. *Mol Cell Biol* 32: 1226-1236, 2012.



Copyright © 2024 Wan et al. This work is licensed under a Creative Commons Attribution-NonCommercial-NoDerivatives 4.0 International (CC BY-NC-ND 4.0) License.